Photometric Properties of Lyα Emitters at z ≈ 4.86 in the COSMOS 2 Square Degree Field

Shioya, Y.; Taniguchi, Y.; Sasaki, S.; Nagao, T.; Murayama, T.; Saito, T.; Ideue, Y.; Nakajima, A.; Matsuoka, K.; Trump, J.; ...

The Astrophysical Journal, 696:546–561, 2009 May 1 doi:10.1088/0004-637X/696/1/546

PHOTOMETRIC PROPERTIES OF Lyα EMITTERS AT $z \approx 4.86$ IN THE COSMOS 2 SQUARE DEGREE FIELD*

Y. Shioya[1], Y. Taniguchi[1], S. S. Sasaki[2,3], T. Nagao[1,3], T. Murayama[3], T. Saito[1], Y. Ideue[2], A. Nakajima[2], K. Matsuoka[2], J. Trump[1,4], N. Z. Scoville[5], D. B. Sanders[6], B. Mobasher[7], H. Aussel[8], P. Capak[5,9], J. Kartaltepe[6], A. Koekemoer[10], C. Carilli[11], R. S. Ellis[5,12], B. Garilli[13], M. Giavalisco[10], M. G. Kitzbichler[14], C. Impey[4], O. LeFevre[15], E. Schinnerer[16], and V. Smolcic[17,18]

[1] Research Center for Space and Cosmic Evolution, Ehime University, Bunkyo-cho, Matsuyama 790-8577, Japan
[2] Graduate School of Science and Engineering, Ehime University, Bunkyo-cho, Matsuyama 790-8577, Japan
[3] Astronomical Institute, Graduate School of Science, Tohoku University, Aramaki, Aoba, Sendai 980-8578, Japan
[4] Steward Observatory, University of Arizona, Tucson, AZ 85721, USA
[5] Department of Astronomy, MS 105-24, California Institute of Technology, Pasadena, CA 91125, USA
[6] Institute for Astronomy, University of Hawaii, 2680 Woodlawn Drive, HI 96822, USA
[7] Department of Physics and Astronomy, University of California, Riverside, CA, 92521, USA
[8] AIM Unité Mixte de Recherche CEA CNRE Université Paris VII UMR n158, France
[9] Spitzer Science Center, California Institute of Technology, Pasadena, CA 91125, USA
[10] Space Telescope Science Institute, 3700 San Martin Drive, Baltimore, MD 21218, USA
[11] National Radio Astronomy Observatory, P.O. Box 0, Socorro, NM 87801-0387, USA
[12] Department of Astrophysics Keble Road, Oxford OX2 3RH, UK
[13] INAF, Istituto di Astrofisica Spaziale e Fisica Cosmica, Sezione di Milano, via Bassini 15, 20133 Milano, Italy
[14] Max-Planck-Institut für Astrophysik, D-85748 Garching bei München, Germany
[15] Laboratoire d'Astrophysique de Marseille, BP 8, Traverse du Siphon, 13376 Marseille Cedex 12, France
[16] Max Planck Institut für Astronomie, Königstuhl 17, Heidelberg, D-69117, Germany
[17] Princeton University Observatory, Princeton, NJ 08544, USA
[18] University of Zagreb, Department of Physics, Bijenicka cesta 32, 10000 Zagreb, Croatia
Received 2008 August 8; accepted 2009 February 2; published 2009 April 16

ABSTRACT

We present results of a survey for Lyα emitters at $z \approx 4.86$ based on optical narrowband ($\lambda_c = 7126$ Å, $\Delta\lambda = 73$ Å) and broadband (B, V, r', i', and z') observations of the Cosmic Evolution Survey field using Suprime-Cam on the Subaru Telescope. We find 79 Lyα emitter (LAE) candidates at $z \approx 4.86$ over a contiguous survey area of 1.83 deg^2, down to the Lyα line flux of 1.47×10^{-17} erg s^{-1} cm^{-2}. We obtain the Lyα luminosity function with a best-fit Schechter parameters of $\log L^* = 42.9^{+0.5}_{-0.3}$ erg s^{-1} and $\phi^* = 1.2^{+8.0}_{-1.1} \times 10^{-4}$ Mpc^{-3} for $\alpha = -1.5$ (fixed). The two-point correlation function for our LAE sample is $\xi(r) = (r/4.4^{+5.7}_{-2.9}\ \mathrm{Mpc})^{-1.90\pm0.22}$. In order to investigate the field-to-field variations of the properties of Lyα emitters, we divide the survey area into nine tiles of $0.^\circ5 \times 0.^\circ5$ each. We find that the number density varies with a factor of $\simeq 2$ from field to field with high statistical significance. However, we find no significant field-to-field variance when we divide the field into four tiles with $0.^\circ7 \times 0.^\circ7$ each. We conclude that at least 0.5 deg^2 survey area is required to derive averaged properties of LAEs at $z \sim 5$, and our survey field is wide enough to overcome the cosmic variance.

Key words: galaxies: distances and redshifts – galaxies: evolution – galaxies: luminosity function, mass function

1. INTRODUCTION

Study of the formation and evolution of galaxies is among the most important topics in modern astrophysics. An essential component of such investigations is the identification of galaxies at the highest redshifts, when most of the galaxies formed, and study of their rest-frame properties. This requires multi-waveband, wide-area and deep surveys of galaxies to provide statistically significant population of these objects. Recently, complementary observations of selected fields by the largest ground-based and space-borne telescopes have made this aim possible by extending this study to $z \sim 7$ and providing statistically large samples of high-redshift galaxies with a significant fraction of them confirmed spectroscopically (see Taniguchi 2008 for a recent review).

To summarize, there are two established techniques to search for high-z galaxy candidates. First, the Lyman break method (i.e., also called drop-out technique) which identifies the continuum break characteristic of Lyα absorption by the intergalactic medium (IGM; Steidel et al. 1996; for a review see Giavalisco 2002). The high-z candidates selected by this technique are called Lyman break galaxies (LBGs). Second, the narrowband imaging technique which aims for detection of galaxies with strong Lyα emission—so-called Lyα emitters (LAEs; Taniguchi et al. 2003a,b for a review). Although both LBGs and LAEs are actively star-forming galaxies, there are systematic differences between them. For example, the stellar populations of LAEs are relatively younger, they have a smaller stellar mass (e.g., Lai et al. 2008), smaller size (e.g., Dow-Hygelund et al. 2007), and are less dusty (e.g., Shapley et al. 2003) compared to the LBGs. These observations imply that the LAEs are likely to be in an earlier star formation phase with respect to LBGs. Furthermore, it is estimated that the average mass of dark matter halos hosting LAEs and LBGs at $z \sim 4$–5 ($\sim 10^{12}\ M_\odot$) are comparable (Ouchi et al. 2004; Kovač et al. 2007), while, at $z \sim 3.1$ ($\sim 10^{11}\ M_\odot$), it is smaller for the LAEs (Gawiser et al. 2007). This implies that the LAEs at $z \sim 3.1$ are likely progenitors of present-day L^* galaxies, whereas the LAEs at $z \sim 4$–5 and LBGs at $z \sim 3$–5 will evolve into present-day galaxies with $L > 2.5L^*$(Gawiser et al. 2007).

* Based on data collected at Subaru Telescope, which is operated by the National Astronomical Observatory of Japan.

To understand differences between the LAEs and LBGs at any given redshift and their properties with look-back time, one needs statistically large and complete samples of these galaxies at different redshifts. Specially for the LAEs, due to technical difficulties in performing narrowband observations, the majority of these surveys are performed over small areas and in selected redshift slices where there are windows to avoid absorption of the lines by the atmosphere. This problem is particularly serious for candidates at higher redshifts where one needs both depth and wide-area coverage to have sufficient number of galaxies and to minimize the cosmic variance.

For the LAEs at $z \sim 5.7$, extensive studies in different fields have been performed, including survey around quasar SDSS J1044−0125 (Ajiki et al. 2003), SSA22 (Hu et al. 2004), GOODS-N and GOODS-S (Ajiki et al. 2006), the Subaru Deep Field (SDF; Shimasaku et al. 2006), the Subaru-XMM Newton Deep Field (SXDF; Ouchi et al. 2005, 2008), and the Cosmic Evolution Survey (COSMOS; Murayama et al. 2007). However, there are only limited surveys of LAEs at other redshifts. This is a serious deficiency in studying evolution of clustering of the LAEs and their rest-frame properties specially if these are expected to evolve to nearby elliptical galaxies (Gawiser et al. 2007).

In this paper, we perform the largest survey of the LAEs at $z \approx 4.86$, covering the entire 2 deg^2 of the COSMOS field (Scoville et al. 2007; Koekemoer et al. 2007). Earlier studies of the LAEs at this redshift revealed the presence of large-scale structures of 20×50 Mpc^2 size (Ouchi et al. 2003; Shimasaku et al. 2003) that are comparable to almost the size of the surveyed area, indicating serious cosmic variance in these data (Shimasaku et al. 2003). The survey performed in this study covers an area of 190×190 Mpc^2 (seven times larger than the survey area of Shimasaku et al. 2003, 2004), large enough to encompass structures of $\sim 50 \times 50$ Mpc^2 size, allowing for proper sampling of the average properties of LAEs at $z \sim 4.9$. Therefore, we are able to examine how the cosmic variance affects the derivation of both the Lyα luminosity functions (LFs) and the clustering properties for the first time.

In the next section, we present our sample selection of LAEs. In Section 3, we discuss the Lyα LF and the clustering properties of our sample. We summarize our results in Section 4. Throughout this paper, magnitudes are given in the AB system. We adopt a flat universe with $\Omega_{\rm matter} = 0.3$, $\Omega_\Lambda = 0.7$, and $H_0 = 70$ km s^{-1} Mpc^{-1}.

2. THE SAMPLE

2.1. The Data

We carried out an optical narrowband (NB711; $\lambda_c = 7126$ Å, $\Delta\lambda = 73$ Å) imaging survey of the entire 2 deg^2 area of the COSMOS field, using the Suprime-Cam on the Subaru Telescope. The NB711 observations were done on 2006 February (Y. Taniguchi et al. 2008, in preparation). The data were reduced using the IMCAT software.[19] Combining the NB711 data with the broadband (B, V, r', i', and z') Suprime-Cam imaging data and i^*-band Mega-Prime/CFHT imaging data already available (Taniguchi et al. 2007; Capak et al. 2007),[20] we identified LAE candidates at $z \approx 4.86$. Details of the narrowband and broadband observations and data reduction are presented by Taniguchi et al. (2007), Y. Taniguchi et al. (2008, in preparation), and Capak et al. (2007).

The FWHMs corresponding to the point-spread functions (PSFs) on the final images are 0.″95 (B), 1.″33 (V), 1.″05 (r'), 0.″95 (i'), 1.″15 (z'), and 0.″79 (NB711). The images were all degraded to a PSF size of 1.″33. The limiting AB magnitudes of the final PSF matched images are: $B = 27.56$, $V = 26.77$, $r' = 26.95$, $i' = 26.49$, $z' = 25.45$, and NB711 = 25.17 for a 3σ detection in a 3″ diameter aperture. We then performed source detection on the original NB711 image using SExtractor (Bertin & Arnouts 1996), followed by photometry over an aperture of 3″ diameter as described in Capak et al. (2007). Similarly, i^*-band (CFHT) magnitudes over the same aperture, are used to identify interlopers consisting of bright galaxies with $i' < 22$.

After subtracting the masked-out regions, the effective survey area is 1.83 deg^2. The redshift coverage of NB711 is $4.83 \leqslant z \leqslant 4.89$ ($\Delta z = 0.06$), giving an effective survey volume of 1.1×10^6 Mpc^3 (comoving).

2.2. Selection of Lyα Emitters at $z \approx 4.86$

In order to select NB711-excess objects efficiently, we first need the magnitude of a frequency-matched continuum. Since the effective frequency of the NB711 filter (421.1 THz) lies between r' (482.8 THz) and i' (394.0 THz) bands, we estimate the frequency-matched continuum, "ri continuum," using the linear combination: $f_{ri} = 0.3 f_{r'} + 0.7 f_{i'}$, where $f_{r'}$ and $f_{i'}$ are the flux densities in r' and i' bands, respectively. This gives a 3σ limiting magnitude of $ri_{\rm lim,3\sigma} = 26.84$ for the continuum (in a 3″ diameter aperture). Since brighter objects with $i' < 22$ are saturated in Subaru images, we use the i^* flux density, f_{i^*}, to calculate the "ri continuum" for such objects, i.e., $f_{ri} = 0.3 f_{r'} + 0.7 f_{i^*}$.

The NB711-excess objects are then selected using the following criteria:

$$ri - \mathrm{NB711} > 0.7, \quad \text{and} \tag{1}$$

$$ri - \mathrm{NB711} > 3\sigma(ri - \mathrm{NB711}), \tag{2}$$

where $3\sigma(ri - \mathrm{NB711}) = -2.5\log(1 - \sqrt{(f_{3\sigma_{\rm NB711}})^2 + (f_{3\sigma_{ri}})^2}/f_{\rm NB711})$.

The first criterion corresponding to an observed equivalent width of EW$_{\rm obs} > 66$ Å, means the flux density in narrowband is twice as large as the flux density of ri continuum. This kind of criterion is conventionally used for LAE survey (e.g., Ouchi et al. 2003; Ajiki et al. 2006; Murayama et al. 2007) to select reliable emitter candidates. Taking account the scatter of the $ri -$NB711 color, we added the second criterion. These two criteria are shown in Figure 1. For objects with $ri < ri_{\rm lim,3\sigma}$, we use the lower-limit value of the NB711 excess, $(ri - \mathrm{NB711})_{\rm low.limit} = ri_{\rm lim,3\sigma} - \mathrm{NB711}$, for our sample selection. We finally select the NB711-excess objects with NB711 < 24.9.

Following the above criteria, we find a total of 1154 NB711-excess objects. These objects include not only LAEs at $z \approx 4.86$, but other low-z interlopers such as Hα, [O III], and [O II] emitting galaxies. In order to distinguish LAEs from low-z interlopers, we compare the observed broadband colors of the LAE candidates with colors that are estimated by using the model spectral energy distribution derived by Coleman et al. (1980), Kinney et al. (1996), and Bruzual & Charlot (2003). Figure 2 shows the $ri -$NB711 versus $r' - i'$ color–color diagram with the predicted colors overlaid. Because of the cosmic transmission (Madau et al. 1996), the $r' - i'$ colors of LAEs are predicted to be redder

[19] IMCAT is distributed by Nick Kaiser at http://www.ifa.hawaii.edu/kaiser/imcat/

[20] http://irsa.ipac.caltech.edu/data/COSMOS/

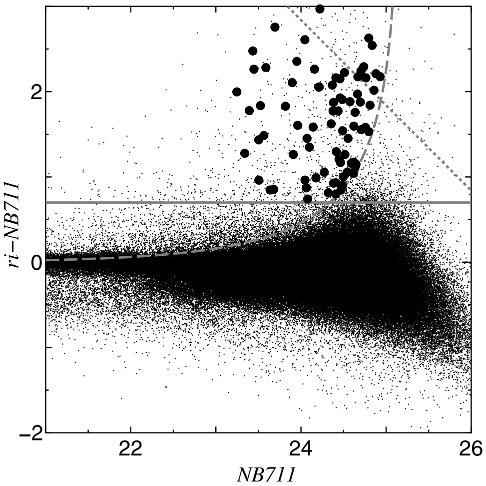

Figure 1. ri − NB711 vs. NB711 diagram for all the NB711 detected sources in COSMOS. The horizontal solid line corresponds to $ri - \mathrm{NB711} = 0.7$. The dashed line show the distribution of the 3σ errors. The dotted line shows the limiting magnitude of ri. Filled circles represent 79 LAE candidates detected here.

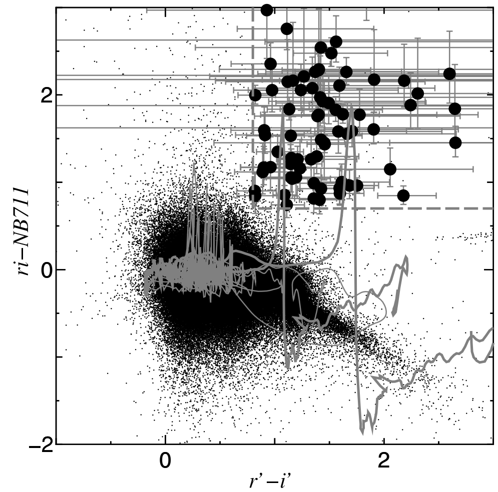

Figure 2. ri − NB711 vs. $r' - i'$ diagram. Thick gray lines show colors of model LAE SEDs, which are calculated with BC03 model (Bruzual & Charlot 2003) with an exponential decay time of τ = 1Gyr and an age of 1 Gyr, corresponding to a cosmic transmission of $0.5\tau_{\mathrm{eff}}$ (left) and τ_{eff} (right) in the formulation of Madau et al. (1996). Luminosity of the Lyα emission is calculated as $L(\mathrm{Ly}\alpha) = 1.2 \times 10^{-11} N_{\mathrm{Lyc}}$, where N_{Lyc} is the ionizing photon production rate (Leitherer & Heckman 1995; Brocklehurst 1971). Thin gray lines show color loci of starburst galaxies (Kinney et al. 1996), typical elliptical, spiral, and irregular galaxies (Coleman et al. 1980) up to $z = 2$.

than low-z emission-line galaxies. Based on results from Figure 2, we added another condition to the selection criteria:

$$r' - i' > 0.8\ . \tag{3}$$

Since the Lyman break is redshifted to ∼5300 Å, the B-band flux of LAEs at $z \approx 4.86$ is expected to be zero. The B-dropout is an effective criterion to distinguish LAEs from low-z interlopers. Here, we must pay attention to the contamination from nearby objects on the sky. If there are objects detected in B band near the LAE and the fluxes from these objects in the aperture are not negligible, the LAE may be misclassified as a low-z interloper. We show B-band images of two of our final LAE candidates in Figure 3. Although there is no object at the position of the emission-line object (center), the B-band magnitude in 3″ diameter aperture is brighter than 27.56 (3σ), because of the contamination from the object that lies at a distance of ∼1″.5 from the center. To avoid the contamination from such nearby objects, we adopt the B-band magnitude measured within the small aperture (0″.5ϕ) in the original image. We therefore add another selection criterion,

$$B_{\mathrm{original}}(0''.5\phi) > 30.09\ , \tag{4}$$

where $B_{\mathrm{original}}(0''.5\phi)$ is the B-band magnitude over a 0″.5 diameter aperture, measured in the original image (i.e., the image before convolving and with a PSF size of 0″.95). The 3σ limiting magnitude for a 0″.5ϕ) aperture in the original image is 30.09.

Based on the added criteria, we can now clearly distinguish LAEs from the low-z interlopers. We finally select a total of 79 LAE candidates at $z \sim 4.86$. The photometric properties of these LAE candidates are listed in Table 1. Their broad- and NB711-band images are presented in Figure 4.

To further check the validity of our photometric selection and their expected redshifts, we extract information of the LAE candidates from the COSMOS spectroscopic catalog. A total of seven LAEs in our final candidate list have spectroscopic redshifts. Figure 5 presents the spectroscopic redshift distribution of these LAEs. This peaks at $z \approx 4.85$ with all the spectroscopic redshifts lying in the range $4.80 < z < 4.85$. This result suggests that our selection criteria work quite well to identify LAEs at $z \approx 4.9$.

2.3. Lyα Luminosity

We estimate the line fluxes for our LAE candidates, F_{L}, using the prescription by Pascual et al. (2001). We express the flux density in each filter band using the line flux, F_{L}, and the continuum flux density, f_{C}:

$$f_{\mathrm{NB}} = f_{\mathrm{C}} + \frac{F_{\mathrm{L}}}{\Delta\mathrm{NB}} \tag{5}$$

$$f_{r'} = f_{\mathrm{C}} \tag{6}$$

$$f_{i'} = f_{\mathrm{C}} + \frac{F_{\mathrm{L}}}{\Delta i'}, \tag{7}$$

where ΔNB and $\Delta i'$ are the effective bandwidths of NB711 and i', respectively. The ri continuum is expressed as

$$f_{ri} = 0.3 f_{r'} + 0.7 f_{i'} = f_{\mathrm{C}} + 0.7\frac{F_{\mathrm{L}}}{\Delta i'}. \tag{8}$$

Using Equations (5) and (8), the line flux, F_{L}, is calculated by

$$F_{\mathrm{L}} = \Delta\mathrm{NB}\frac{f_{\mathrm{NB}} - f_{ri}}{1 - 0.7(\Delta\mathrm{NB}/\Delta i')}. \tag{9}$$

The limiting line flux of our survey is 1.47×10^{-17} erg s^{-1}. Since the response curve is not square in shape, the observed flux of Lyα emission for a fixed Lyα luminosity depends on the redshift. On average, the observed flux is underestimated by a factor of 0.81, which is calculated by

$$\frac{\int_{\lambda_c-\Delta\lambda/2}^{\lambda_c+\Delta\lambda/2} R(\lambda)d\lambda}{\int_{\lambda_c-\Delta\lambda/2}^{\lambda_c+\Delta\lambda/2} d\lambda} = 0.81\ ,$$

where $R(\lambda)$ is a response function normalized by the maximum value. We therefore apply correction statistically for the filter response by $F_{\mathrm{cor}}(\mathrm{Ly}\alpha) = F_{\mathrm{L}} \times 1.24$. Finally, we estimate the Lyα luminosity as $L(\mathrm{Ly}\alpha) = 4\pi d_{\mathrm{L}}^2 F_{\mathrm{cor}}(\mathrm{Ly}\alpha)$. In this procedure, we assume that all the LAEs are located at $z = 4.86$ ($d_{\mathrm{L}} = 45.1$ Gpc), the redshift corresponding to the central wavelength of our NB711 filter.

Table 1
A List of Lyα Emitter Candidates

#	R.A. (deg)	Decl. (deg)	r' (mag)	i' (mag)	ri (mag)	NB711 (mag)	z' (mag)	$\log L(\mathrm{Ly}\alpha)$ (erg s^{-1})	$\log L_\nu$(1540 Å) (erg s^{-1} Hz^{-1})	M_{UV} (mag)	EW$_0$ (Å)
1	150.68983	1.598039	28.85	26.54	26.87	24.86	25.95	42.68	28.80	−20.4	46
2	150.58466	1.528353	26.26	25.13	25.36	23.52	25.40	43.20	29.02	−21.0	90
3	150.43377	1.584748	27.49	26.38	26.61	24.46	> 26.64	42.85	< 28.52	> −19.7	>127
4	150.47017	1.527121	27.85	26.69	26.92	24.76	26.28	42.73	28.67	−20.1	69
5	150.12679	1.606008	27.15	25.63	25.91	23.43	25.61	43.28	28.94	−20.7	131
6	150.19137	1.514911	25.95	25.13	25.32	24.47	24.79	42.64	29.26	−21.6	14
7	149.42627	1.570369	27.34	25.94	26.21	24.44	> 26.64	42.83	< 28.52	> −19.7	>121
8	149.50750	1.569846	26.40	24.72	25.01	24.05	25.06	42.85	29.15	−21.3	30
9	150.72870	1.654431	27.26	26.02	26.27	24.22	> 26.64	42.94	< 28.52	> −19.7	>156
10	150.69867	1.658967	99.00	27.04	27.42	24.80	> 26.64	42.74	< 28.52	> −19.7	>98
11	150.69845	1.643227	27.19	25.73	26.00	24.55	24.98	42.75	29.19	−21.4	22
12	150.44771	1.639259	26.33	24.16	24.48	23.64	24.31	42.98	29.46	−22.0	20
13	150.21979	1.647579	27.64	25.97	26.26	24.71	25.67	42.70	28.91	−20.7	36
14	149.92387	1.706955	27.91	26.99	27.19	24.22	> 26.64	42.98	< 28.52	> −19.7	>171
15	149.86911	1.741172	27.83	25.18	25.52	24.07	25.43	42.94	29.01	−20.9	51
16	149.81740	1.738043	26.33	25.43	25.63	24.46	25.87	42.73	28.83	−20.5	47
17	149.85339	1.702846	28.17	26.76	27.03	24.74	> 26.64	42.75	< 28.52	> −19.7	>100
18	149.81761	1.638761	26.26	25.23	25.45	24.10	25.25	42.91	29.08	−21.1	41
19	149.47913	1.713145	26.26	24.90	25.17	24.18	24.82	42.81	29.25	−21.5	21
20	150.77783	1.795379	27.63	25.85	26.15	24.38	25.44	42.85	29.00	−20.9	42
21	150.43713	1.821238	27.16	25.26	25.57	23.96	24.83	43.00	29.25	−21.5	34
22	150.39265	1.852772	30.47	26.36	26.74	24.51	> 26.64	42.84	< 28.52	> −19.7	>122
23	150.31602	1.848847	26.35	24.94	25.21	24.41	24.73	42.65	29.29	−21.6	14
24	149.98396	1.914333	27.61	26.12	26.39	24.49	> 26.64	42.82	< 28.52	> −19.7	>119
25	149.76505	1.835950	26.46	25.04	25.31	24.38	24.49	42.71	29.38	−21.9	13
26	149.82192	1.826156	27.56	26.12	26.39	24.46	> 26.64	42.83	< 28.52	> −19.7	>122
27	149.70144	1.880336	29.66	25.88	26.26	24.38	25.73	42.86	28.89	−20.6	56
28	149.43575	1.958916	25.53	24.38	24.62	23.34	24.16	43.20	29.51	−22.2	29
29	150.52280	2.053999	28.66	26.82	27.13	23.87	> 26.64	43.13	< 28.52	> −19.7	>240
30	150.44155	2.045647	25.92	24.17	24.47	23.50	24.13	43.07	29.53	−22.2	21
31	149.80258	1.976421	28.37	26.13	26.46	24.58	25.48	42.78	28.99	−20.9	37
32	149.47068	2.112708	28.53	27.11	27.38	24.84	> 26.64	42.72	< 28.52	> −19.7	>94
33	149.49438	2.111401	27.52	26.13	26.39	24.64	> 26.64	42.75	< 28.52	> −19.7	>100
34	149.50653	2.059920	26.21	24.78	25.05	23.56	25.14	43.15	29.12	−21.2	63
35	149.42625	1.971732	27.00	25.60	25.87	23.59	25.36	43.21	29.04	−21.0	89
36	150.75362	2.237688	27.53	26.18	26.45	24.37	26.27	42.88	28.67	−20.1	97
37	150.74435	2.216502	25.70	24.59	24.82	24.08	24.31	42.76	29.45	−22.0	12
38	150.23097	2.219221	27.93	26.37	26.65	24.04	> 26.64	43.04	< 28.52	> −19.7	>196
39	150.17687	2.162903	27.02	26.05	26.26	24.21	> 26.64	42.95	< 28.52	> −19.7	>157
40	149.96795	2.258172	27.64	26.05	26.34	24.76	26.26	42.68	28.68	−20.1	60
41	150.01739	2.146056	26.51	24.88	25.17	23.39	25.62	43.25	28.93	−20.7	124
42	149.83435	2.270296	26.92	25.37	25.65	23.82	25.58	43.08	28.95	−20.8	81
43	150.68548	2.422582	26.74	25.83	26.03	24.49	25.59	42.78	28.94	−20.8	41
44	150.48986	2.405317	26.14	24.93	25.17	23.91	25.16	42.97	29.11	−21.2	43
45	150.34351	2.380535	26.92	26.01	26.22	24.62	26.54	42.74	28.56	−19.8	89
46	150.17116	2.443712	27.53	25.48	25.79	24.65	25.27	42.66	29.07	−21.1	23
47	149.95843	2.414291	29.20	26.60	26.95	24.70	26.49	42.76	28.58	−19.9	89
48	149.86004	2.390346	27.06	26.09	26.31	23.95	> 26.64	43.07	< 28.52	> −19.7	>208
49	149.62681	2.428601	31.96	26.72	27.11	24.93	25.84	42.66	28.84	−20.5	40
50	149.51027	2.301385	27.33	26.22	26.45	23.69	26.34	43.19	28.64	−20.0	208
51	150.72903	2.584166	26.45	25.56	25.76	24.64	25.67	42.65	28.91	−20.7	33
52	150.78495	2.573355	26.58	25.42	25.66	24.62	25.31	42.64	29.06	−21.0	23
53	150.75115	2.481606	28.43	26.25	26.57	24.41	> 26.64	42.87	< 28.52	> −19.7	>133
54	150.24314	2.530345	27.07	25.42	25.71	23.45	25.44	43.26	29.00	−20.9	108
55	150.13505	2.486044	26.83	25.21	25.50	24.50	25.22	42.68	29.09	−21.1	23
56	149.89657	2.527743	26.57	25.42	25.66	24.45	26.08	42.75	28.75	−20.3	59
57	149.75765	2.572967	28.44	26.53	26.84	24.67	25.54	42.77	28.96	−20.8	38
58	149.87223	2.497300	27.31	25.72	26.00	23.90	25.50	43.07	28.98	−20.9	74
59	149.60335	2.612591	26.85	25.52	25.78	24.52	26.03	42.73	28.77	−20.3	55
60	149.58816	2.521003	27.14	25.43	25.73	24.14	25.28	42.93	29.07	−21.1	43
61	149.46094	2.563734	27.24	26.09	26.33	24.80	25.71	42.66	28.90	−20.6	35
62	150.80329	2.730062	26.73	25.50	25.75	24.59	25.90	42.68	28.82	−20.5	43
63	150.76442	2.688660	25.39	24.31	24.53	23.68	23.91	42.96	29.62	−22.4	13
64	150.43973	2.720629	26.24	25.09	25.33	24.27	25.30	42.78	29.06	−21.1	32

Table 1
(Continued)

#	R.A. (deg)	Decl. (deg)	r' (mag)	i' (mag)	ri (mag)	NB711 (mag)	z' (mag)	$\log L(\mathrm{Ly}\alpha)$ (erg s^{-1})	$\log L_\nu(1540$ Å$)$ (erg s^{-1} Hz^{-1})	M_{UV} (mag)	EW$_0$ (Å)
65	150.30282	2.772591	26.65	25.06	25.34	24.41	24.81	42.70	29.26	−21.5	16
66	150.30023	2.666173	28.11	26.84	27.09	24.88	$>$ 26.64	42.69	$<$ 28.52	$>$ −19.7	$>$87
67	150.28152	2.651694	27.53	26.16	26.42	24.16	$>$ 26.64	42.98	$<$ 28.52	$>$ −19.7	$>$170
68	150.29721	2.634812	26.25	24.65	24.94	24.06	25.12	42.82	29.13	−21.2	29
69	149.94445	2.704370	26.02	25.20	25.39	24.49	25.79	42.66	28.86	−20.6	37
70	149.78731	2.678302	26.12	24.67	24.94	23.50	24.88	43.16	29.23	−21.5	52
71	149.66107	2.739789	26.23	24.87	25.14	24.32	24.66	42.69	29.31	−21.7	14
72	149.72632	2.664706	99.00	25.59	25.98	24.35	$>$ 26.64	42.85	$<$ 28.52	$>$ −19.7	$>$126
73	149.43064	2.784033	28.95	26.30	26.65	24.81	$>$ 26.64	42.69	$<$ 28.52	$>$ −19.7	$>$87
74	149.41782	2.735198	26.83	25.45	25.71	24.41	$>$ 26.64	42.78	$<$ 28.52	$>$ −19.7	$>$107
75	149.44796	2.694757	26.55	25.36	25.60	24.54	24.89	42.68	29.22	−21.5	17
76	150.31928	2.864155	27.78	26.37	26.64	24.66	$>$ 26.64	42.76	$<$ 28.52	$>$ −19.7	$>$102
77	150.23253	2.849228	99.00	26.19	26.58	24.70	$>$ 26.64	42.74	$<$ 28.52	$>$ −19.7	$>$97
78	149.80660	2.861745	25.88	25.05	25.24	23.25	24.83	43.33	29.25	−21.5	71
79	149.43851	2.902153	26.54	25.58	25.79	24.62	25.48	42.67	28.99	−20.9	29

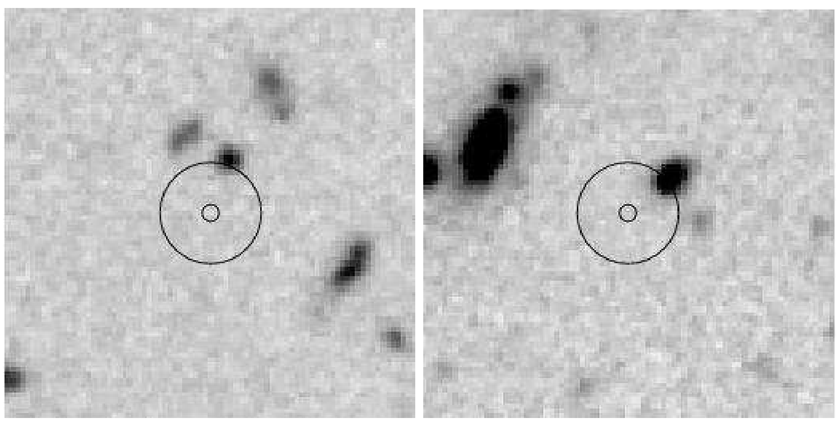

Figure 3. *B*-band images of our LAE candidates 16 and 44. Each box is 12″ on a side (north is up and east is left). The diameter of a small (large) circle is 0″.5 (3″). In both cases, there are no counter parts in the center, although the flux within 3″ diameter aperture is larger than 3σ because of the contamination from nearby objects.

3. RESULTS AND DISCUSSION

3.1. Spatial Distribution

Figure 6 presents the spatial distribution of our 79 LAE candidates at $z \sim 4.86$. The contours of local surface density ($2\bar{\Sigma}$, where $\bar{\Sigma}$ is the averaged surface density over the whole field, 43 deg^{-2}) are shown in the figure. The local surface density at position (x, y) is the density averaged over the circle centered at (x, y), whose radius is determined as the angular distance to the third nearest neighbors. There are 10 overdensity regions in the field. A typical size of the large overdensity region is $0^{\circ}\!.4 \times 0^{\circ}\!.2$ (50×25 Mpc^2), being similar to those found by Shimasaku et al. (2003) and Ouchi et al. (2005).

To check for field-to-field variation, we divide the survey area into nine subfields, each corresponding to a sky area of $0^{\circ}\!.5 \times 0^{\circ}\!.5$ ($63\times$ 63 Mpc^2; Figure 6). The number density of the LAEs in each subfield is summarized in Table 2. We find significant field-to-field variations among the nine subfields by a factor of $\simeq$2. This means that the typical scale of the large-scale structure is comparable to the size of the subfield, that is consistent with the size of the overdensity regions found in the above. The field-to-field variations found here, agree with those for LAEs at $z \approx 5.7$, independently estimated in the SXDF (Ouchi et al. 2008) and with theoretical predictions using the cosmological hydrodynamic simulations (Nagamine et al. 2008) for the fields of $\sim$0.2 deg^2. Our finding suggests that the derived properties of LAEs from the survey with a small survey area (smaller than $0^{\circ}\!.5 \times 0^{\circ}\!.5$) may be affected by the cosmic variance.

Table 2
The Number Density of LAEs in the Nine Subfields of $0^{\circ}\!.5 \times 0^{\circ}\!.5$

	East (deg^{-2})	Middle (deg^{-2})	West (deg^{-2})
North	29.6 ± 12.1	52.0 ± 15.7	64.3 ± 17.8
Middle	30.9 ± 12.6	28.0 ± 11.4	45.3 ± 15.1
South	59.5 ± 17.9	28.0 ± 11.4	53.1 ± 16.0

We also divide the survey area into four subfields, each corresponding to a sky area of $0^{\circ}\!.7 \times 0^{\circ}\!.7$ (95×95 Mpc^2). We find 21, 21, 19, and 18 LAEs in northeastern (NE), northwestern (NW), southwestern (SW), and southeastern (SE) quadrant, respectively. This means that the typical scale of the large-scale structure is smaller than the size of the subfield. Our finding suggests that the derived properties of LAEs

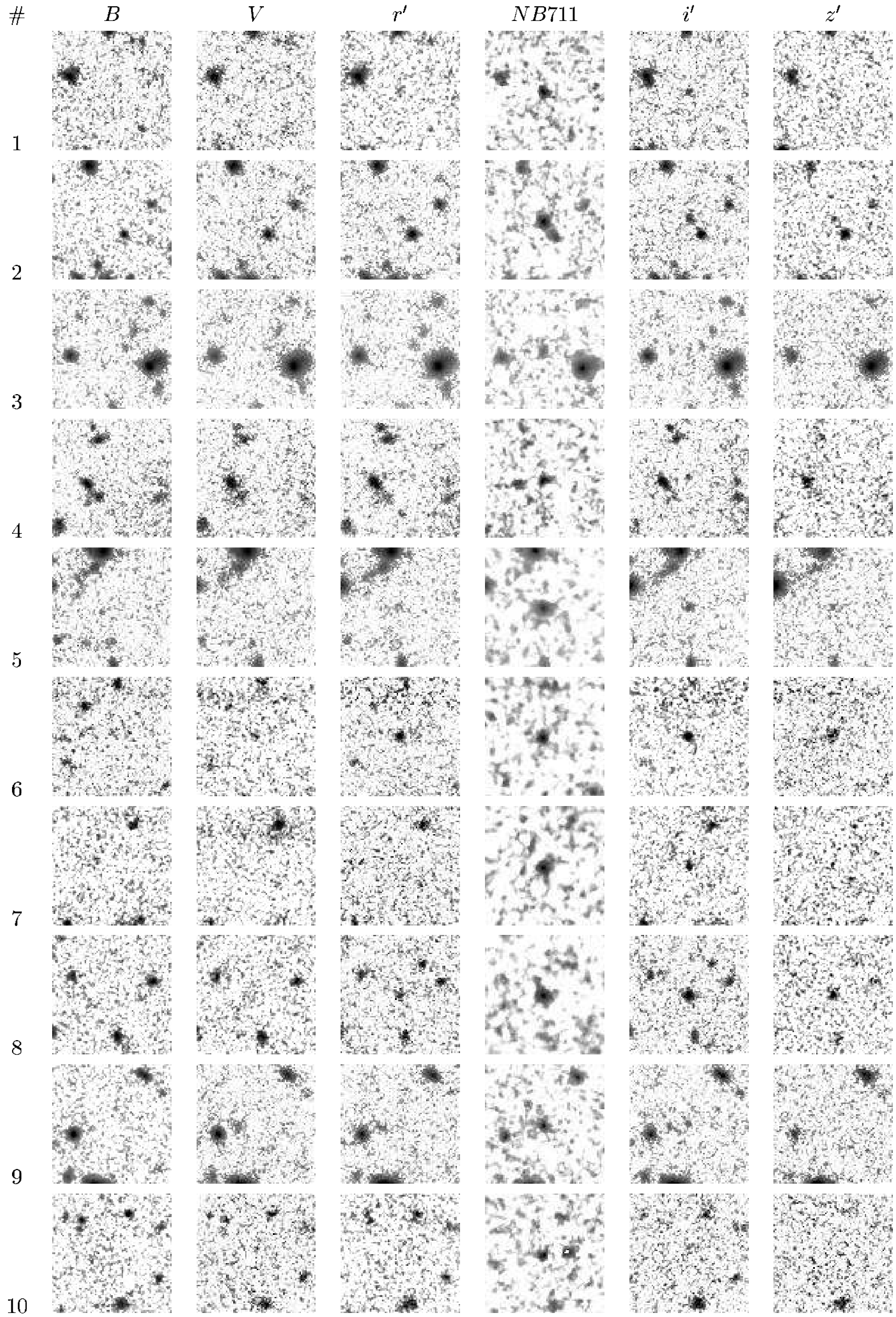

Figure 4. Broadband and NB711 images of our LAE candidates at $z \approx 4.9$. Each box is 12″ on a side (north is up and east is left).

from the survey with a large survey area (larger than $0^\circ\!.7 \times 0^\circ\!.7$) are considered to be averaged ones over the universe at $z \sim 5$.

3.2. Lyα Luminosity Function

The rest-frame Lyα LF for our sample of LAEs at $z \approx 4.86$ is presented in Figure 7. The LF is measured as

$$\Phi(\log L_i) = \frac{N_i}{V_{\rm co}}, \tag{10}$$

where $V_{\rm co}$ is the comoving volume of 1.1×10^6 Mpc^3 ($4.83 \leqslant z \leqslant 4.89$) and N_i is a number of LAEs within $\log L_i \pm \frac{1}{2}\Delta \log L$. We use $\Delta \log L({\rm Ly}\alpha) = 0.2$. We fit the rest-frame Lyα LF with the Schechter function (Schechter 1976) using parametric maximum likelihood estimator (Sandage et al. 1979). Since the characteristic luminosity (L^*) and the faint-end slope (α) of the Schechter LFs are not independent, we perform the fit by fixing α to -1, -1.5, and -2. Our best-fit Schechter parameters are summarized in Table 3. For comparison, we also plot the Lyα LF for a sample selected by Ouchi et al. (2003). Their survey

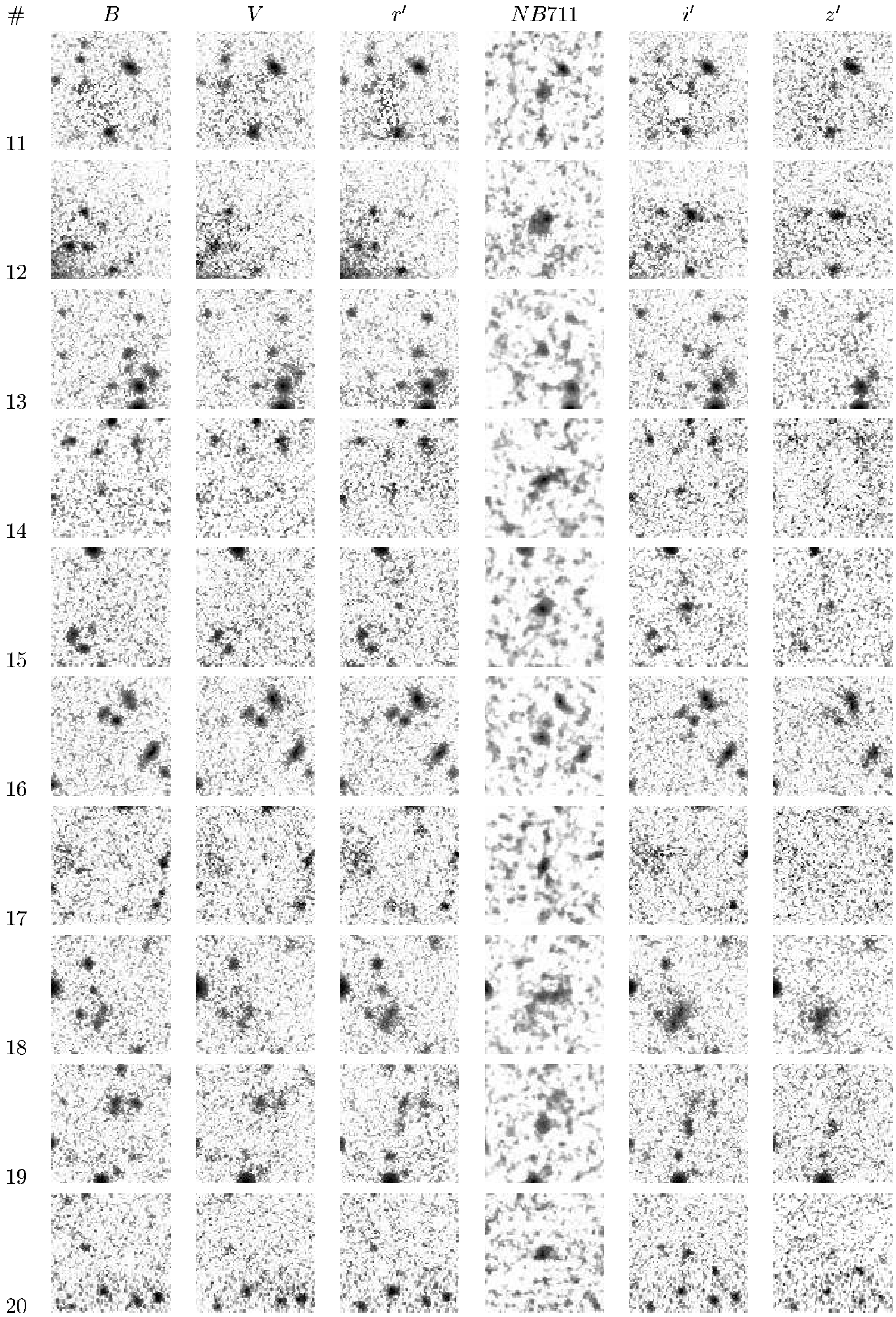

Figure 4. (Continued)

was performed by using the same narrowband filter (NB711), for smaller field (543 arcmin^2) and deeper (down to NB711 = 26.0) than ours. Although our sample does not include low-luminosity LAEs and their sample does not include LAEs at the luminous end, our Lyα LF is consistent with that of Ouchi et al. (2003) for the range of $42.8 \leqslant \log L(\mathrm{Ly}\alpha) \leqslant 43.2$.

Since the filter response curve of NB711 is not box-shaped, the narrowband magnitude of LAEs of a fixed Lyα luminosity

Table 3
Best-Fit Schechter Parameters for Lyα Luminosity Functions

α (Fixed)	$\log L^*_{\mathrm{Ly}\alpha}$ (erg s^{-1})	ϕ^* ($\times 10^{-4}$ Mpc^{-3})
−1.0	$42.82^{+0.39}_{-0.28}$	$1.41^{+6.73}_{-1.09}$
−1.5	$42.91^{+0.49}_{-0.31}$	$1.22^{+8.02}_{-1.05}$
−2.0	$43.00^{+0.70}_{-0.37}$	$0.82^{+9.98}_{-0.77}$

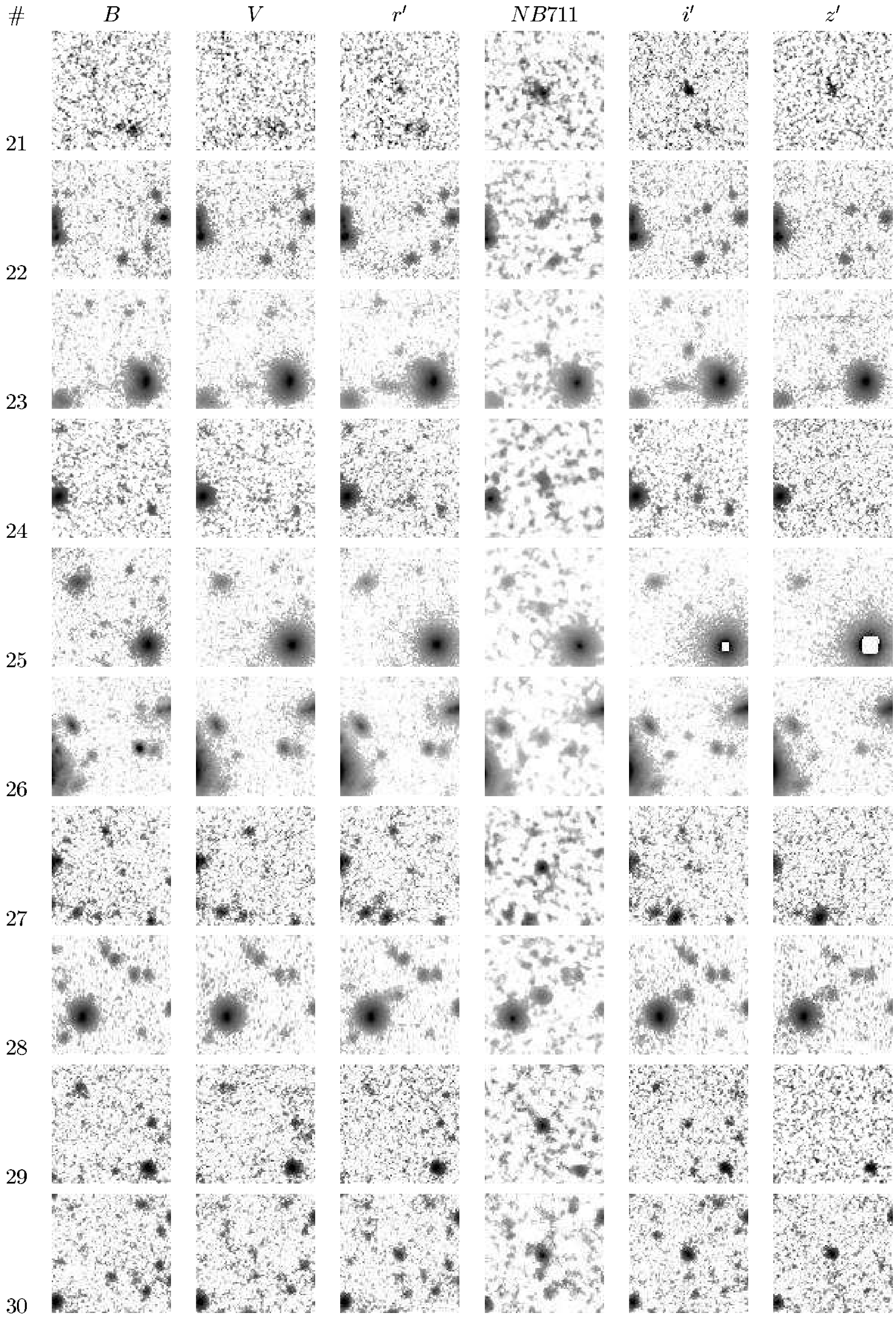

Figure 4. (Continued)

varies as a function of the redshift. The selection function of LAEs in terms of the equivalent width also changes with the redshift (Shimasaku et al. 2006; Ouchi et al. 2008). We check the validity of the Lyα LF derived above. In order to examine whether or not we can reconstruct an input Lyα LF by our selection criteria and an estimation of Lyα flux, we performed the Monte Carlo simulations that are similar to those made by Shimasaku et al. (2006). First, we generate a mock catalog of LAEs with a set of the Schechter parameters (α, ϕ^*, L^*) and a Gaussian distribution function of EW, $f(\mathrm{EW}_0)d\mathrm{EW}_0 \propto \exp(-\mathrm{EW}_0^2/2\sigma_{\mathrm{EW}})d\mathrm{EW}_0$. We adopt four σ_{EW} values: $\sigma_{\mathrm{EW}} = 50$, 100, 200, and 400 Å. We uniformly distribute them in comoving space over $4.7 < z < 5.1$. Next, we select Lyα emitters and evaluate the Lyα LF applying the method written above for the mock catalog. We show results of our simulations in Figure 8. We confirm that the Lyα LF we evaluate is very close to the input LF. We conclude that the simple method we adopted is valid for evaluating the Lyα LF.

We plot the Lyα LFs from the four subfields in Figure 7 (left panel). Those LFs are consistent within their errors. We also

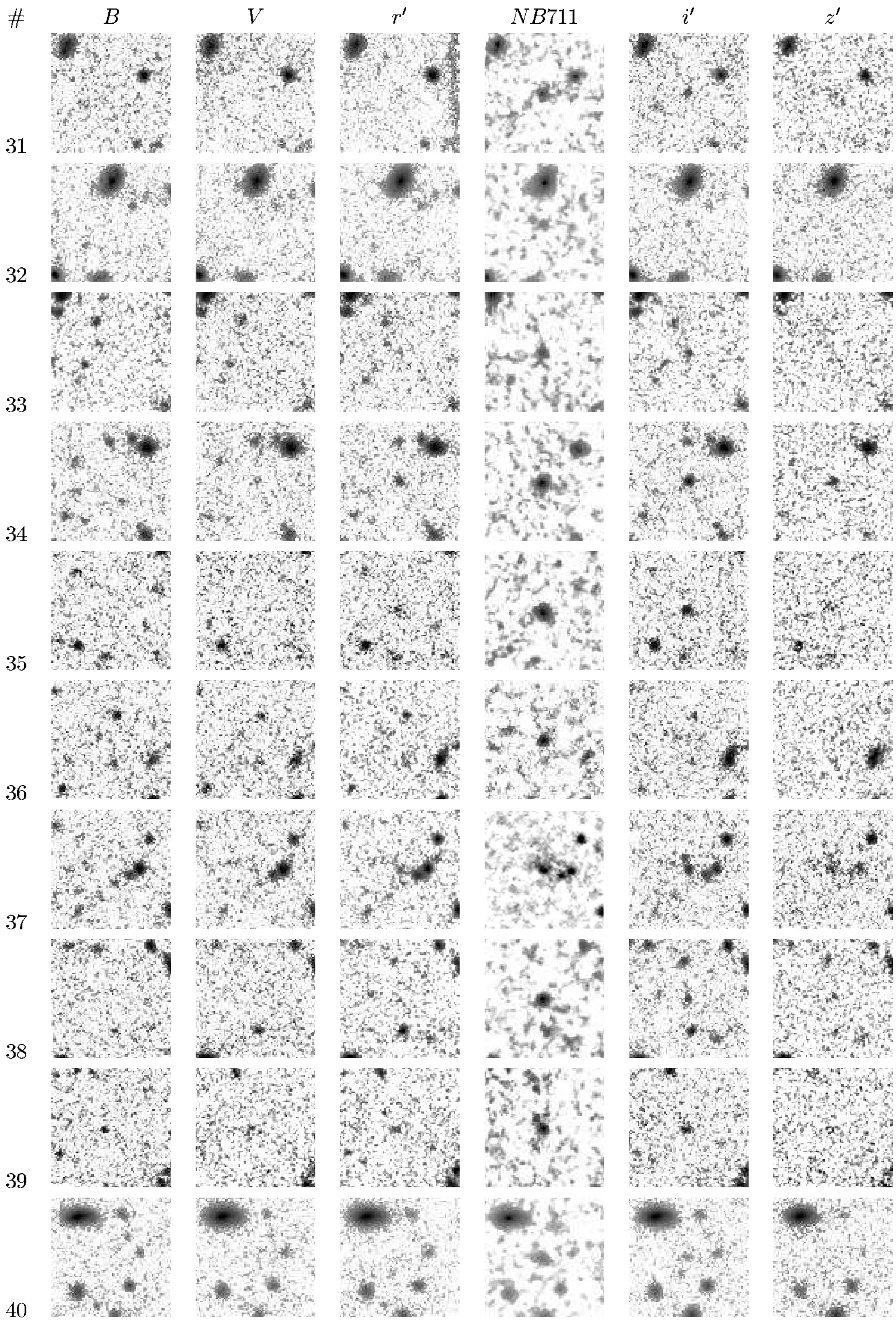

Figure 4. (Continued)

summarize the best-fit Schechter parameters for four subfields in Table 4. Although the field-to-field variation of ϕ^* is a factor of 4, each value exists within the error in Table 3. In Figure 7 (right panel), we compare our results with other LAE surveys in the redshift range $z \sim 3.1$–6.6. Although various surveys have slightly different selection criteria, most of the Lyα LFs are similar to each other. We then find that estimated Lyα LF is very similar to those at $3.1 \leqslant z \leqslant 5.7$ within errors. This result supports the little evolution of Lyα LFs in the range of $3 < z < 6$ (Tran et al. 2004; van Breukelen et al. 2005; Shimasaku et al. 2006; Ouchi et al. 2008).

3.3. Equivalent Widths

Figure 9 shows the distribution of $\mathrm{EW}_0(\mathrm{Ly}\alpha)$. To measure the rest-frame UV continuum flux, we use the z'-band data as the fluxes at i' band are affected by Lyα emission. For objects fainter than 1σ in the z' band, we calculate the upper limit of the UV luminosity, $L_\nu(\mathrm{UV})$, and the lower limit of the rest-frame equivalent width, $\mathrm{EW}_0(\mathrm{Ly}\alpha)$. The $\mathrm{EW}_0(\mathrm{Ly}\alpha)$ distribution is similar to those in previous studies of LAEs at $z \sim 3$–6 (e.g., Shimasaku et al. 2006; Dawson et al. 2007; Ouchi et al. 2008; Gronwall et al. 2007), with the mean rest-frame Lyα

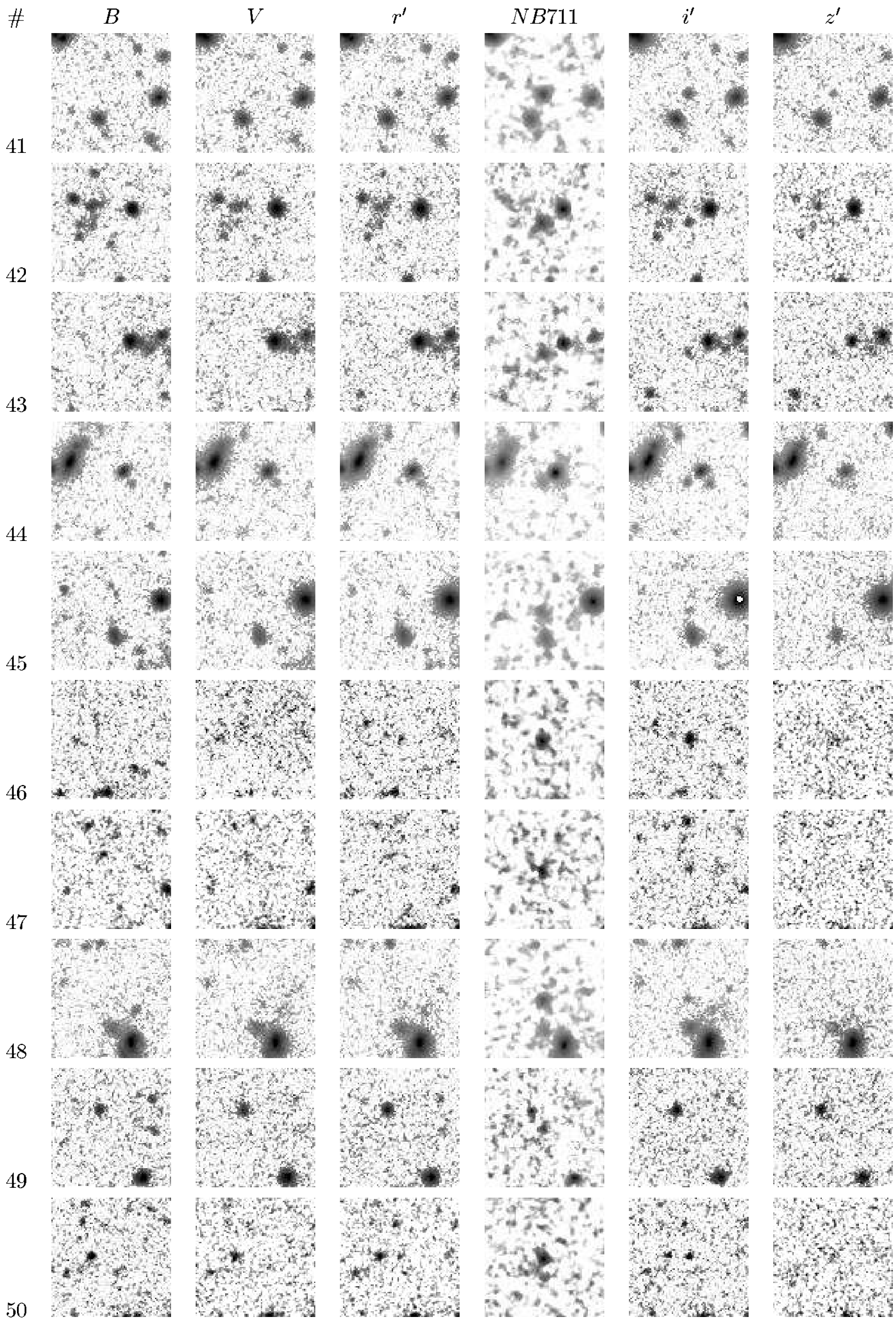

Figure 4. (Continued)

equivalent widths of the sample smaller than 200 Å. There is no LAE with $\mathrm{EW_0(Ly\alpha)} > 250$ Å in our sample, although the rest-frame Lyα equivalent widths of 23 of the LAEs in our sample (29%) are lower limits. Taking account of a predicted $\mathrm{EW_0(Ly\alpha)}$ for starburst galaxies, 300 Å for young starburst (age $\leqslant 10^6$ years) and 100 Å for old starburst (age $\sim 10^8$ years) (Malhotra & Rhoads 2002), we consider that there is no peculiar object in our sample. Figure 10 shows the relation between $\mathrm{EW_0(Ly\alpha)}$ and M_{UV}. There is no object with $\mathrm{EW_0(Ly\alpha)} > 80$ Å in the UV-bright ($M_{\mathrm{UV}} < -21.5$) sample. Although the number of UV-bright LAEs is small and the uncertainties on $\mathrm{EW_0}$s for UV-faint objects are large, this trend is similar to that found for LBGs and LAEs at $z \sim$ 5–6 (Ando et al. 2006; Shimasaku et al. 2006; Ouchi et al. 2008). We conclude that our sample shows the "average" picture of bright LAEs at $z \sim 5$.

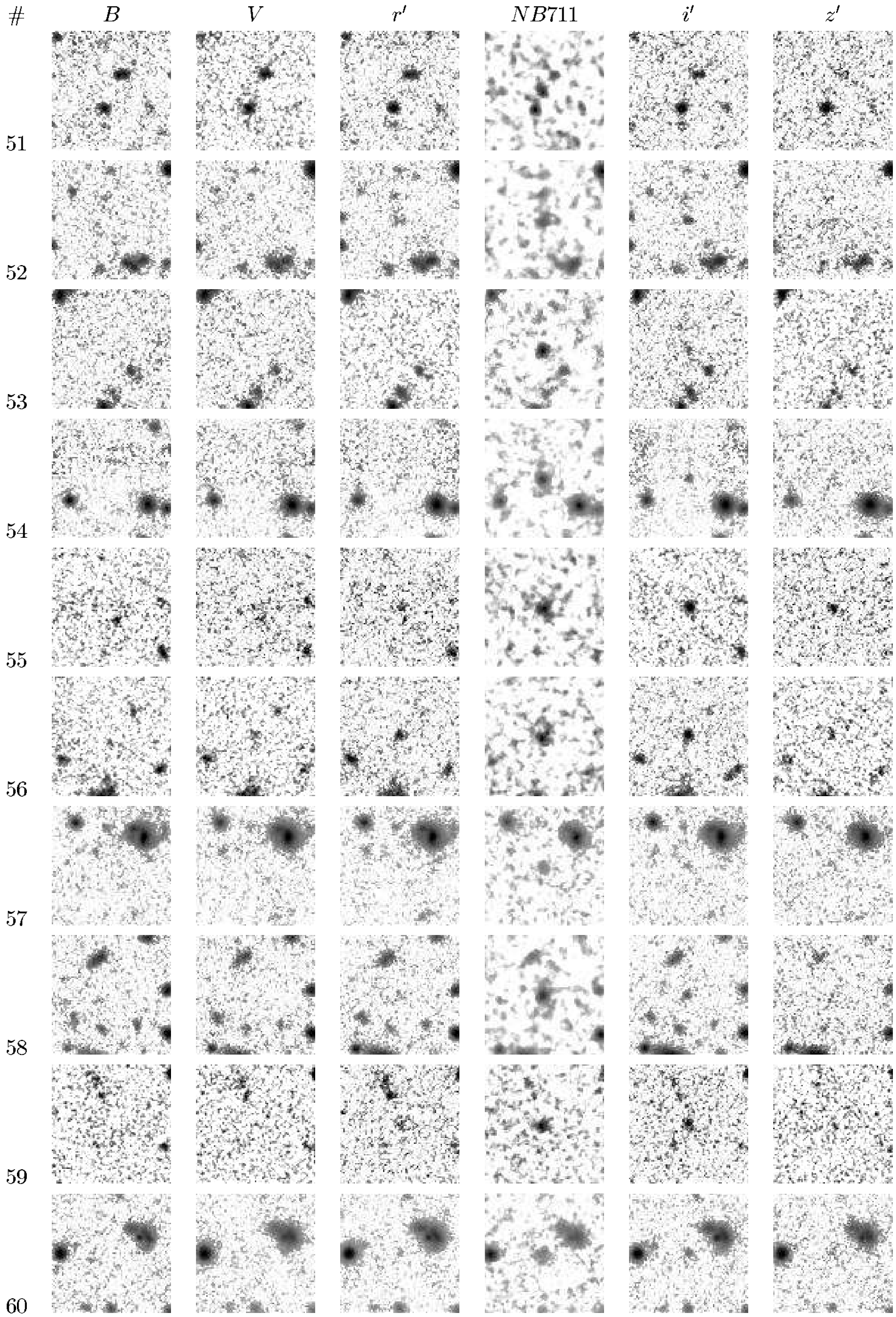

Figure 4. (Continued)

3.4. UV Luminosity Function

Figure 11 shows UV LF of our sample (black symbols). The UV LFs of LAEs estimated in the four subfields are consistent within errors. Figure 11 also include the UV LF of LBGs at $z \sim 5$ (Yoshida et al. 2006) and LAEs at $z \sim 3.1$, 3.7, and 5.7 (Ouchi et al. 2008). The shape of our UV LF seems different from those of previous works and is not fitted by Schechter function, since a detection limit of rest-frame equivalent width, $\mathrm{EW}_0(\mathrm{Ly}\alpha)$, depends on M_{UV}, e.g., $\mathrm{EW}_0(\mathrm{Ly}\alpha) > 11$ Å at $M_{\mathrm{UV}} < -21.5$ and $\mathrm{EW}_0(\mathrm{Ly}\alpha) > 57$ Å at $M_{\mathrm{UV}} = -20$ (see Figure 10). As a reference, we overlay the result of our Monte Carlo simulation for $\alpha = -1.5$ and $\sigma_{\mathrm{EW}} = 100$ Å: dotted line shows input UV LF for $\mathrm{EW}_0(\mathrm{Ly}\alpha) > 11$ Å and solid line shows output UV LF. This result also shows that our UV LF is considered to be complete for LAE with $\mathrm{EW}_0 > 11$ Å for $M_{\mathrm{UV}} < -21.5$. We therefore concentrate the number density at $M_{\mathrm{UV}} < -21.5$.

First, we compare our UV LF with that of LBGs at $z \sim 5$. The number density of our LAEs is comparable to that of LBGs at $z \sim 5$ at $M_{\mathrm{UV}} \sim -22\%$ and $\sim$20%–25% at $M_{\mathrm{UV}} = -21.5$.

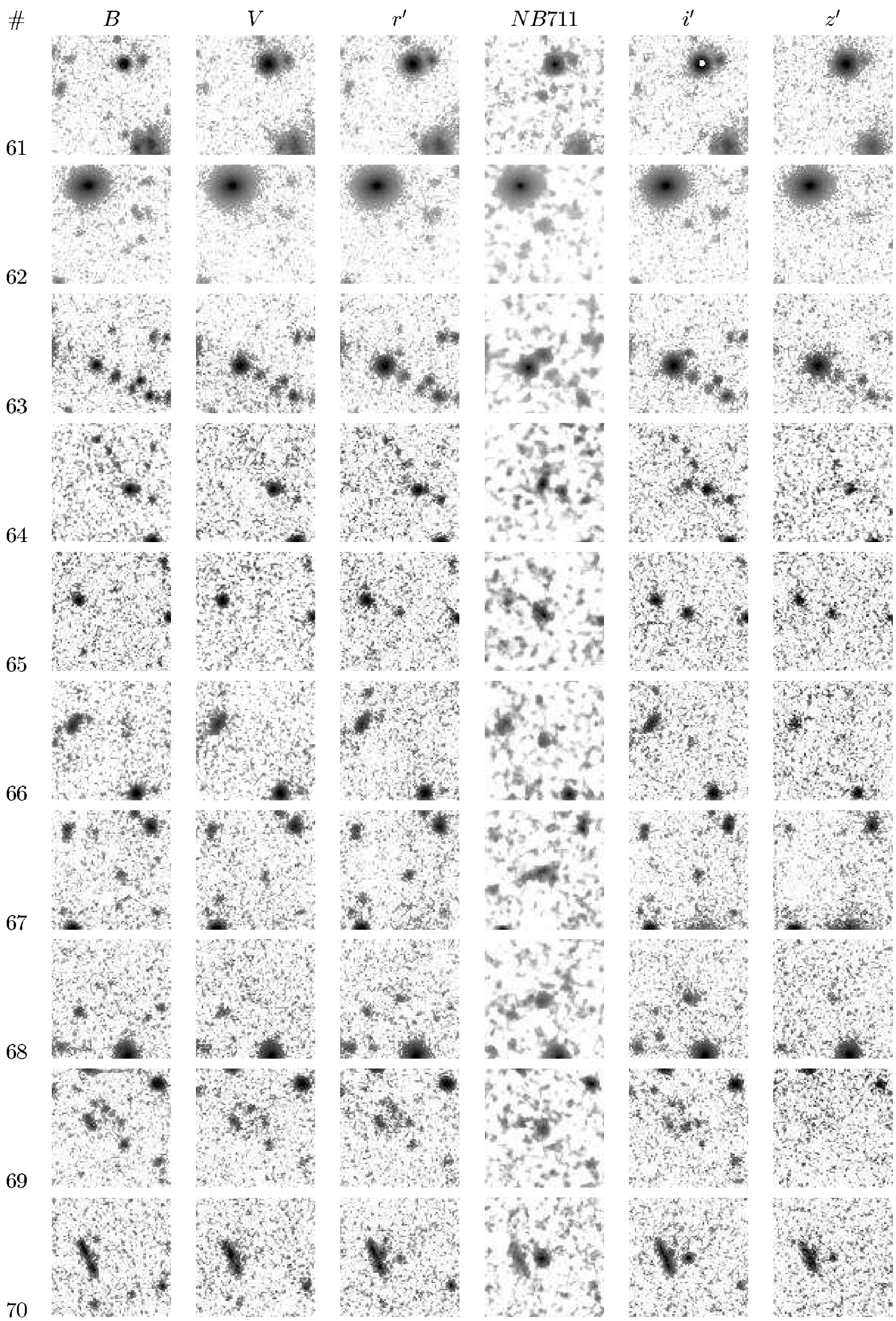

Figure 4. (Continued)

Ouchi et al. (2008) pointed out that the ratio of number densities of LAEs to those of LBGs is $\sim$10% at $z = 3$–4 and >50% at $z = 5.7$. Our result implies that the ratio of the number density of LAEs to that of LBGs becomes larger with redshift from $z = 4$ to 5. Next, we compare our UV LF with those of LAEs at different redshifts. Figure 12 shows the number density of LAEs at $M_{\rm UV} = -21.5$ as a function of z. The number density of our LAEs at $M_{\rm UV} = -21.5$ is comparable to that of LAEs at $z \sim 5.7$, while larger than those of LAEs at $z \sim 3.1$ and 3.7. The number density of UV-bright LAEs ($M_{\rm UV} < -21.5$) increases an order of magnitude with redshift from $z = 4$ to 5. Since it is likely that the LAEs are star-forming galaxies in an earlier star formation phase, our findings imply that the initial active star formation phase occurs mainly beyond $z = 5$.

3.5. Clustering Properties

We found the large-scale structure of LAEs of $0^{\circ}\!.4 \times 0^{\circ}\!.2$ in Section 3.1. In order to perform a more quantitative study of the clustering properties of the LAEs at $z \sim 4.86$, we derive their

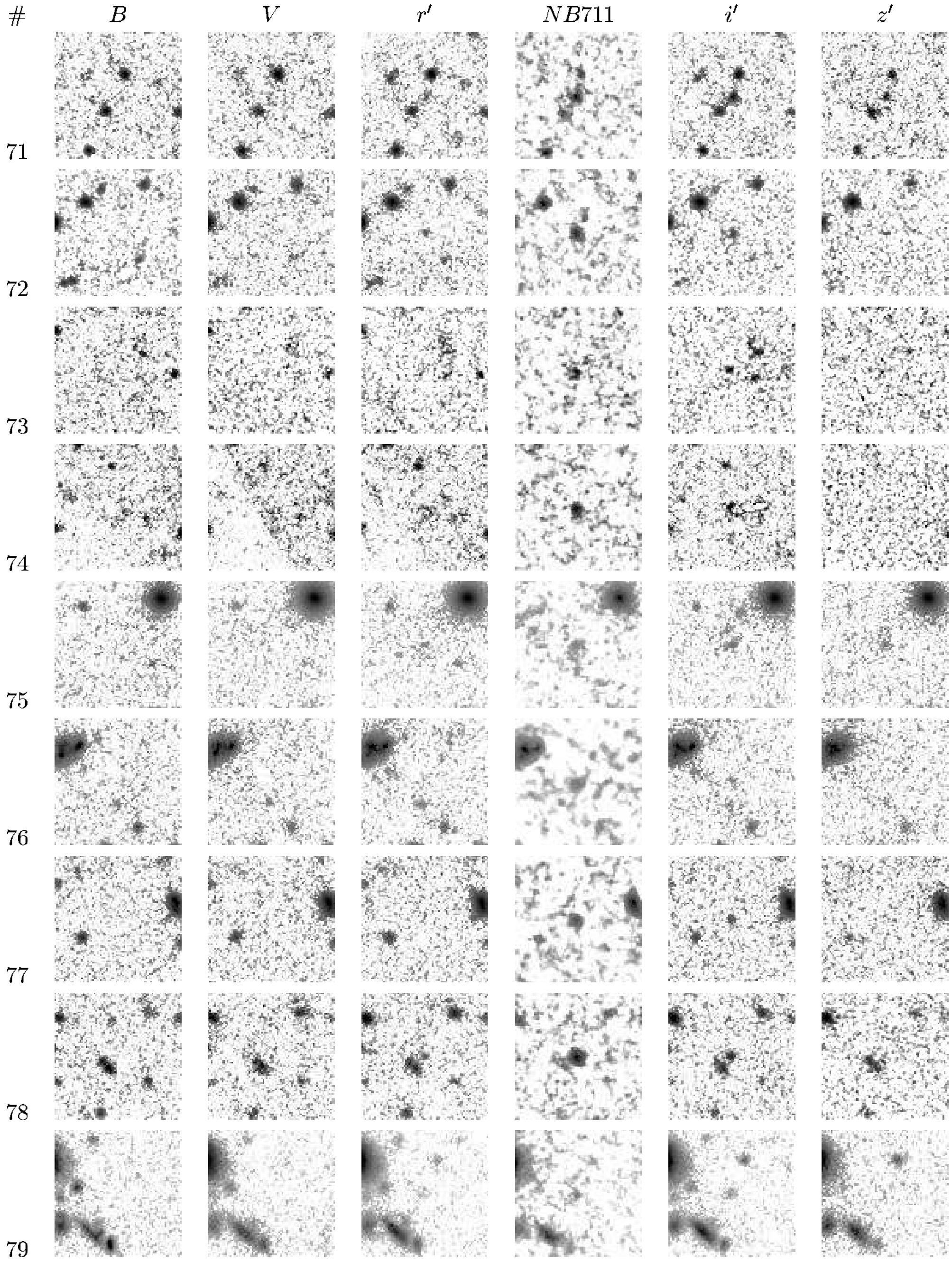

Figure 4. (Continued)

angular two-point correlation function (ACF), $w(\theta)$, using the estimator defined by Landy & Szalay (1993),

$$w(\theta) = \frac{DD(\theta) - 2DR(\theta) + RR(\theta)}{RR(\theta)}, \tag{11}$$

where $DD(\theta)$, $DR(\theta)$, and $RR(\theta)$ are normalized numbers of galaxy–galaxy, galaxy–random, and random–random pairs, respectively. The random sample here consists of 100,000 sources with the same geometrical constraints as the galaxy sample. The observed ACF is fitted well by a single power law: $w(\theta) = 0.021^{+0.025}_{-0.011}\,\theta^{-0.90\pm0.22}$ (Figure 13). The correlation length, r_0, is calculated from the ACF through Limber's equation (e.g., Peebles 1980), assuming a top-hat redshift distribution centered on $z = 4.86 \pm 0.03$. We estimated the r_0 corresponding to our sample of LAEs as $r_0 = 4.4^{+5.7}_{-2.9}$ Mpc. The two-point correlation function is thus written as $\xi(r) = (r/4.4^{+5.7}_{-2.9}\,\mathrm{Mpc})^{-1.90\pm0.22}$. This agrees well with results from other works at similar redshifts, e.g., $r_0 = 5.0 \pm 0.4$ for $z \simeq 4.9$ (Ouchi et al. 2003); $r_0 = 4.57 \pm 0.60$ for $z \simeq 4.5$ (Kovač et al. 2007).

Also shown in Figure 13 are the ACFs for the LAEs in the four subfields. We detect strong clustering signals in small scale ($\theta \leqslant 50'$) for NE, SW, and SE subfields, with the NW subfield showing no clustering signals at any angular separations. Although this may imply the presence of a cosmic variance on the clustering properties similar to that found in a previous study (Shimasaku et al. 2004), taking account of large uncertainties of ACFs, we consider that there are no significant field-to-field variations among the four subfields.

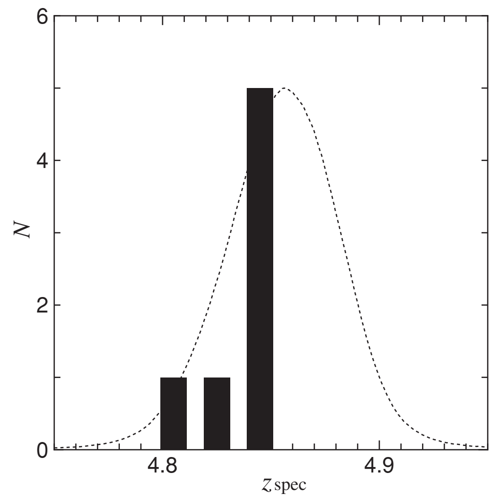

Figure 5. Spectroscopic redshift distribution of our LAE sample (seven LAEs). The dotted line shows the response function of the NB711 band.

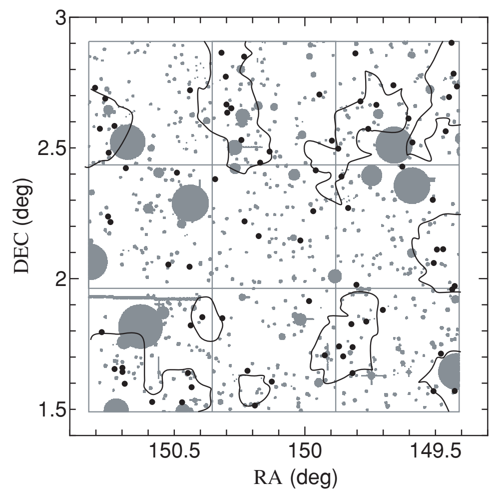

Figure 6. Spatial distributions of LAEs (black filled circles). The shaded regions show the areas masked out for the detection. The contours show the local surface density of the LAEs, drawn at the level twice as high as the average over the field, 43 deg^{-2}.

Table 4
Best-Fit Schechter Parameters for Lyα Luminosity Functions for Each Subfield

α (Fixed)	Subfield	$\log L^*_{\mathrm{Ly}\alpha}$ (erg s^{-1})	ϕ^* ($\times 10^{-4}$ Mpc^{-3})
−1.0	NE	42.79	0.85
	NW	42.76	3.0
	SW	42.92	0.84
	SE	42.83	1.4
−1.5	NE	42.87	0.78
	NW	42.84	2.7
	SW	43.02	0.68
	SE	42.91	1.2
−2.0	NE	42.97	0.56
	NW	42.94	2.0
	SW	43.15	0.40
	SE	43.02	0.83

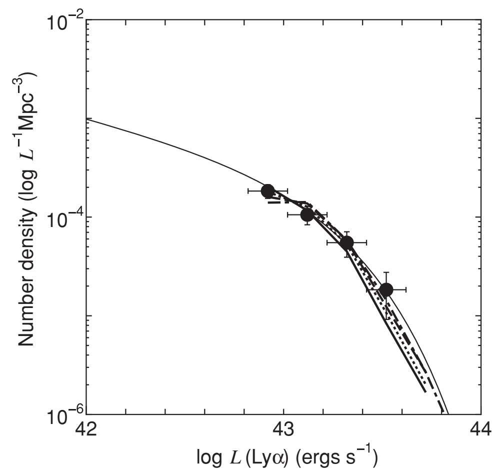

Figure 8. Results of our Monte Carlo simulations for $\alpha = -1.5$. The derived Lyα luminosity functions are shown as thick solid, thick dotted, thick dashed, and thick dash-dotted lines for the case of $\sigma_{\mathrm{EW}} = 50$, 100, 200, and 400 Å, respectively. These luminosity functions are similar to the input Schechter function (thin solid line).

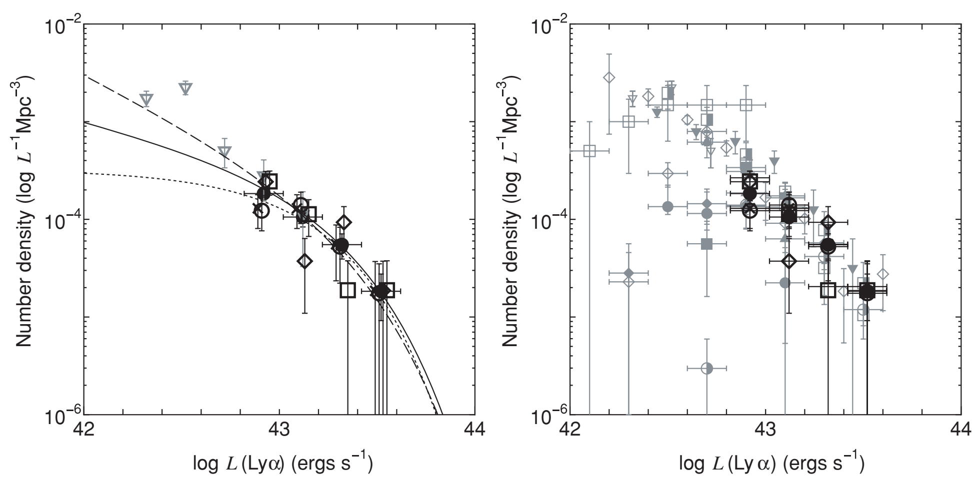

Figure 7. Left: the Lyα LF of our LAE sample (black symbols). The Lyα LF for the whole sample is shown with filled circles. The dotted, solid, and dashed lines show the best-fit Schechter functions for the whole sample for $\alpha = -1$, -1.5, and -2, respectively. The Lyα LFs for different quadrants are shown with boxes, diamonds, circles, and crosses for the NE, NW, SW, and SE subfields, respectively. For comparison, the Lyα LF derived by Ouchi et al. (2003) is shown with inverse triangles. Right: same as the left panel, compared with other surveys (gray symbols): for LAEs at $z \sim 3.1$ (circles: Ouchi et al. 2008), $z \sim 3.4$ (boxes: Cowie & Hu 1998), $z \sim 3.7$ (triangles: Ouchi et al. 2008), $z \sim 4.9$ (inverse triangles: Ouchi et al. 2003), $z \sim 5.7$ (filled circles: Rhoads & Malhotra 2001; filled boxes: Ajiki et al. 2003; filled diamonds: Hu et al. 2004; filled triangles: Ajiki et al. 2006; filled inverse triangles: Shimasaku et al. 2006; half-filled circles: Murayama et al. 2007; half-filled boxes: Ouchi et al. 2008), and $z \sim 6.6$ (diamonds: Taniguchi et al. 2005).

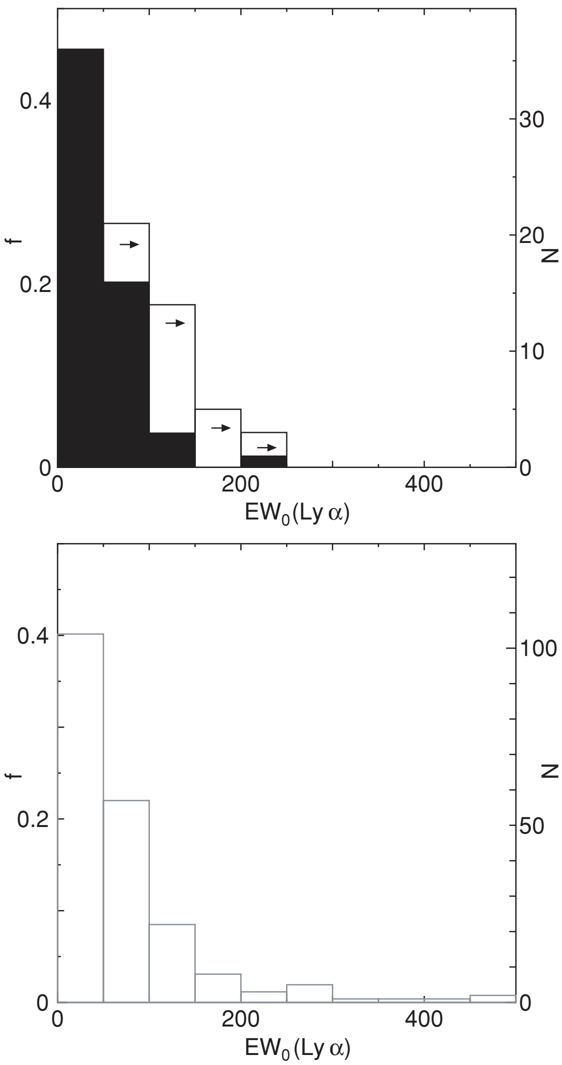

Figure 9. Top: distribution of the rest-frame Lyα equivalent widths. Filled bars show the LAEs with the continuum detected above 1σ. The open bars show the LAEs with no continuum detection. Bottom: distribution of the rest-frame Lyα equivalent widths of the LAEs at $z \sim 3.1$ obtained by Gronwall et al. (2007).

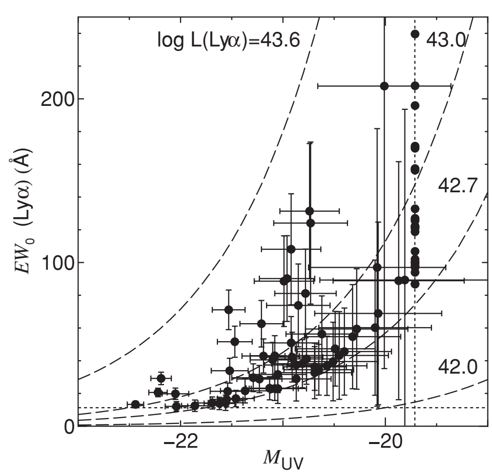

Figure 10. Rest-frame EWs of Lyα lines vs. absolute magnitude at rest-frame 1540 Å for our sample of LAEs at $z \sim 4.9$. The dashed lines show loci of the constant Lyα luminosities for $\log L(\mathrm{Ly}\alpha) = 43.6$, 43.0, and 42.0, where $L(\mathrm{Ly}\alpha)$ is in units of erg s^{-1}. The dotted line corresponds to $M_{\mathrm{UV}} = -19.71$ which is the rest-UV absolute magnitude corresponding to the z'-band limiting magnitude (1σ).

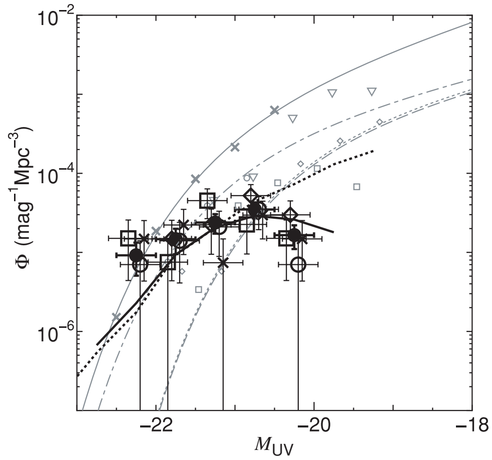

Figure 11. Rest-frame UV LF of our LAE sample (black symbols). The UV LF for our whole sample is shown with filled circles. The UV LFs for different quadrants of the COSMOS field are shown with black boxes, black diamonds, black circles, and black crosses for the NE, NW, SW, and SE fields, respectively. The results of our Monte Carlo simulation for $\alpha = -1.5$ and $\sigma_{\mathrm{EW}} = 100$ Å are overlaid: the dotted line shows the input UV LF with $\mathrm{EW}_0(\mathrm{Ly}\alpha) > 13$ Å and the solid line shows the output UV LF. For comparison, we show UV LFs from the previous surveys (gray symbols): LAEs at $z \sim 4.9$ (inverse triangles: Ouchi et al. 2003), LBGs at $z \sim 5$ (crosses and solid line: Yoshida et al. 2006), LAEs at $z = 3.1$ (open diamonds and dotted line: Ouchi et al. 2008), $z = 3.7$ (open boxes and dashed line: Ouchi et al. 2008), and $z = 5.7$ (open circle and dot-dashed line: Ouchi et al. 2008).

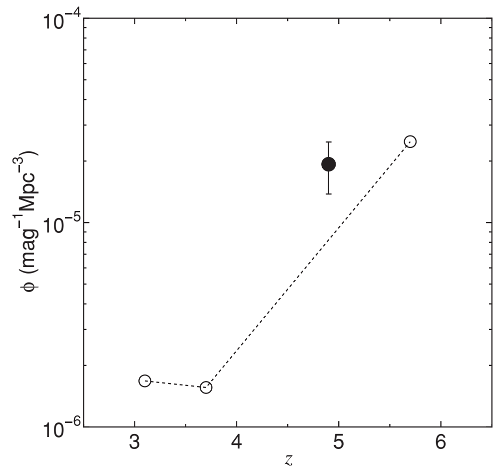

Figure 12. Number density of LAEs at $M_{\mathrm{UV}} = -21.5$ as a function of z. Our data point is shown with filled circles with a error bar. The open circles show the number densities derived by Ouchi et al. (2008).

4. SUMMARY

We have performed the largest survey to date for Lyα emitters at $z \approx 4.86$, using narrowband (NB711) imaging technique in the COSMOS 2 deg^2 field. We have found a total of 79 Lyα emission-line galaxy candidates. For seven LAE candidates with available spectroscopic data, we have confirmed that our criteria for selecting LAEs at $z \approx 4.86$ are working well. Our results and conclusions are summarized below.

1. We have found a field-to-field variation of the number density of LAEs as large as a factor of $\simeq 2$ among the nine subfields with $0^\circ\!.5 \times 0^\circ\!.5$. On the other hand, the number density of LAEs for four subfields with $0^\circ\!.7 \times 0^\circ\!.7$ is consistent within an error. This finding is consistent with the scale of large-scale structure we found, 50×25 Mpc^2. We conclude that at least 0.5 deg^2 survey area is required to derive averaged properties of

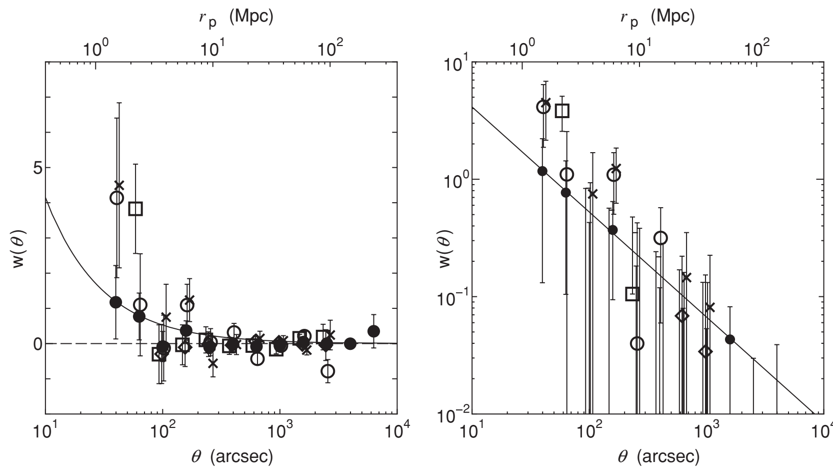

Figure 13. Left: angular two-point correlation function (ACF) of our LAE sample. Filled circles show the ACF for the whole sample. The ACFs for different quadrants are shown with boxes, diamonds, circles, and crosses for the NE, NW, SW, and SE subfield, respectively. Right: same as the left panel with $w(\theta)$ shown in logarithmic scale.

LAEs at $z \sim 5$, and our survey field is wide enough to overcome the cosmic variance.

2. The Lyα LF is well fitted by a Schechter function with best-fit Schechter parameters: $\log L^* = 42.91^{+0.49}_{-0.31}$ erg s^{-1} and $\phi^* = 1.22^{+8.02}_{-1.05} \times 10^{-4}$ Mpc^{-3} for $\alpha = -1.5$ (fixed). The two-point correlation function is well fitted by a power law, $w(\theta) = 0.021^{+0.025}_{-0.011}\theta^{-0.90\pm0.22}$, giving $\xi(r) = (r/4.4^{+5.7}_{-2.9}\ \mathrm{Mpc})^{-1.9}$.

3. We have derived the UV LF of LAEs. The number densities of our LAEs at $M_{\mathrm{UV}} = -21.5$ are similar to those of LAEs at $z \sim 5.7$ while larger than those of LAEs at $z \sim 3$–4. The number density of UV-bright LAEs increases an order of magnitude with redshift from $z \sim 4$ to 5.

The *HST* COSMOS Treasury program was supported through NASA grant *HST*-GO-09822. We greatly acknowledge the contributions of the entire COSMOS collaboration consisting of more than 70 scientists. We thank Masami Ouchi for useful discussion and the anonymous referee for valuable comments. We also thank the Subaru Telescope staff for their invaluable help. This work was financially supported in part by the JSPS (Nos. 15340059 and 17253001).

REFERENCES

Ajiki, M., Mobasher, B., Taniguchi, Y., Shioya, Y., Nagao, T., Murayama, T., & Sasaki, S. S. 2006, ApJ, 638, 596
Ajiki, M., et al. 2003, AJ, 126, 2091
Ando, M., Ohta, K., Iwata, I., Akiyama, M., Aoki, K., & Tamura, N. 2006, ApJ, 645, L9
Ando, M., Ohta, K., Iwata, I., Watanabe, C., Tamura, N., Akiyama, M., & Aoki, K. 2004, ApJ, 610, 635
Bertin, E., & Arnouts, S. 1996, A&AS, 117, 393
Brocklehurst, M. 1971, MNRAS, 153, 471
Bruzual, A. G., & Charlot, S. 2003, MNRAS, 344, 1000
Capak, P., et al. 2007, ApJS, 172, 99
Coleman, G. D., Wu, C.-C., & Weedman, D. W. 1980, ApJS, 43, 393
Cowie, L. L., & Hu, E. M. 1998, AJ, 115, 1319
Dawson, S., et al. 2007, ApJ, 671, 1227
Dow-Hygelund, C. C., et al. 2007, ApJ, 660, 47
Gawiser, E., et al. 2007, ApJ, 671, 278
Giavalisco, M. 2002, ARA&A, 40, 579
Gronwall, C., et al. 2007, ApJ, 667, 79
Hu, E. M., et al. 2004, AJ, 127, 563
Kinney, A. L., et al. 1996, ApJ, 467, 38
Koekemoer, A. M., et al. 2007, ApJS, 172, 196
Kovač, K., Somerville, R. S., Rhoads, J. E., Malhotra, S., & Wang, J. 2007, ApJ, 668, 15
Lai, K., et al. 2008, ApJ, 674, 70
Landy, S. D., & Szalay, A. S. 1993, ApJ, 412, 64
Leitherer, C., & Heckman, T. M. 1995, ApJS, 96, 9
Madau, P., Ferguson, H. C., Dickinson, M. E., Giavalisco, M., Steidel, C. C., & Fruchter, A. 1996, MNRAS, 283, 1388
Malhotra, S., & Rhoads, J. E. 2002, ApJ, 565, L71
Murayama, T., et al. 2007, ApJS, 172, 523
Nagamine, K., Ouchi, M., Springel, V., & Hernquist, L. 2008, arXiv:0802.0228
Ouchi, M., et al. 2003, ApJ, 582, 60
Ouchi, M., et al. 2004, ApJ, 611, 685
Ouchi, M., et al. 2005, ApJ, 620, L1
Ouchi, M., et al. 2008, ApJS, 176, 301
Pascual, S., Gallego, J., Aragón-Salamanca, A., & Zamorano, J. 2001, A&A, 379, 798
Peebles, P. J. E. 1980, The Large-Scale Structure of the Universe, (Princeton, NJ: Princeton Univ. Press)
Rhoads, J. E., & Malhotra, S. 2001, ApJ, 563, L5
Sandage, A., Tammann, G. A., & Yahil, A. 1979, ApJ, 232, 352
Schechter, P. 1976, ApJ, 203, 297
Scoville, N., et al. 2007, ApJS, 172, 1
Shapley, A. E., Steidel, C. C., Pettini, M., & Adelberger, K. L. 2003, ApJ, 588, 65
Shimasaku, K., et al. 2003, ApJ, 586, L111
Shimasaku, K., et al. 2004, ApJ, 605, L93
Shimasaku, K., et al. 2006, PASJ, 58, 313
Steidel, C. C., Giavalisco, M., Pettini, M., Dickinson, M., & Adelberger, K. L. 1996, ApJ, 462, L17
Taniguchi, Y. 2008, in IAU Symp. 250, Massive Stars as Cosmic Engine, ed. F. Bresolin, P. Crowther, & J. Puls (Cambridge: Cambridge Univ. Press), 429
Taniguchi, Y., et al. 2003a, JKAS, 36, 123
Taniguchi, Y., et al. 2003b, JKAS, 36, 283, erratum
Taniguchi, Y., et al. 2005, PASJ, 57, 165
Taniguchi, Y., et al. 2007, ApJS, 172, 9
Tran, K.-V. H., Lilly, S. J., Crampton, D., & Brodwin, M. 2004, ApJ, 612, L89
van Breukelen, C., Jarvis, M. J., & Venemans, B. P. 2005, MNRAS, 359, 895
Yoshida, M., et al. 2006, ApJ, 653, 988

The Astrophysical Journal, 700:899–900, 2009 July 20
doi:10.1088/0004-637X/700/1/899

ERRATUM: "PHOTOMETRIC PROPERTIES OF Lyα EMITTERS AT $z \approx 4.86$ IN THE COSMOS 2 SQUARE DEGREE FIELD" (2009, ApJ, 696, 546)

Y. Shioya[1], Y. Taniguchi[1], S. S. Sasaki[2,3], T. Nagao[1,3], T. Murayama[3], T. Saito[1], Y. Ideue[2], A. Nakajima[2], K. Matsuoka[2], J. Trump[1,4], N. Z. Scoville[5], D. B. Sanders[6], B. Mobasher[7], H. Aussel[8], P. Capak[5,9], J. Kartaltepe[6], A. Koekemoer[10], C. Carilli[11], R. S. Ellis[5,12], B. Garilli[13], M. Giavalisco[10], M. G. Kitzbichler[14], C. Impey[4], O. LeFevre[15], E. Schinnerer[16], and V. Smolcic[17,18]

[1] Research Center for Space and Cosmic Evolution, Ehime University, Bunkyo-cho, Matsuyama 790-8577, Japan
[2] Graduate School of Science and Engineering, Ehime University, Bunkyo-cho, Matsuyama 790-8577, Japan
[3] Astronomical Institute, Graduate School of Science, Tohoku University, Aramaki, Aoba, Sendai 980-8578, Japan
[4] Steward Observatory, University of Arizona, Tucson, AZ 85721, USA
[5] Department of Astronomy, MS 105-24, California Institute of Technology, Pasadena, CA 91125, USA
[6] Institute for Astronomy, University of Hawaii, 2680 Woodlawn Drive, HI 96822, USA
[7] Department of Physics and Astronomy, University of California, Riverside, CA 92521, USA
[8] AIM Unité Mixte de Recherche CEA CNRE Université Paris VII UMR n158, France
[9] *Spitzer* Science Center, California Institute of Technology, Pasadena, CA 91125, USA
[10] Space Telescope Science Institute, 3700 San Martin Drive, Baltimore, MD 21218, USA
[11] National Radio Astronomy Observatory, P.O. Box 0, Socorro, NM 87801-0387, USA
[12] Department of Astrophysics, Keble Road, Oxford OX2 3RH, UK
[13] INAF, Istituto di Astrofisica Spaziale e Fisica Cosmica, Sezione di Milano, via Bassini 15, 20133 Milano, Italy
[14] Max-Planck-Institut für Astrophysik, D-85748 Garching bei München, Germany
[15] Laboratoire d'Astrophysique de Marseille, BP 8, Traverse du Siphon, 13376 Marseille Cedex 12, France
[16] Max Planck Institut für Astronomie, Königstuhl 17, D-69117 Heidelberg, Germany
[17] Princeton University Observatory, Princeton, NJ 08544, USA
[18] University of Zagreb, Department of Physics, Bijenicka cesta 32, 10000 Zagreb, Croatia

Due to an error in processing the data, we have published wrong values of EW_0 in Table 1 in the original paper, published 2009 April 16. The true values are derived by the multiplication of 0.83 to the values in Table 1 in the original paper. As a result, Figures 9 and 10 are incorrect in the original paper. The correct versions of Figures 9 (top) and 10 are presented here.

The Lyα luminosity functions (LFs) of our sample in Figures 7 and 8 are corrected for the absorption by intergalactic neutral hydrogen as in Figure 4(a) in Ouchi et al. (2003, ApJ, 582, 60). The correct caption to Figure 7 is "the Lyα LF of our sample that is corrected for the absorption by intergalactic neutral hydrogen as Ouchi et al. (2003)" instead of "the Lyα LF of our sample."

These do not change any discussion in the text.

We thank Masakazu A. R. Kobayashi for bringing these errors to our attention.

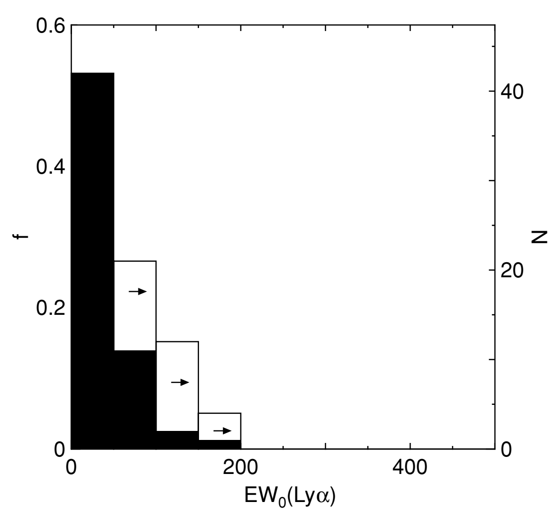

Figure 9. (Top)

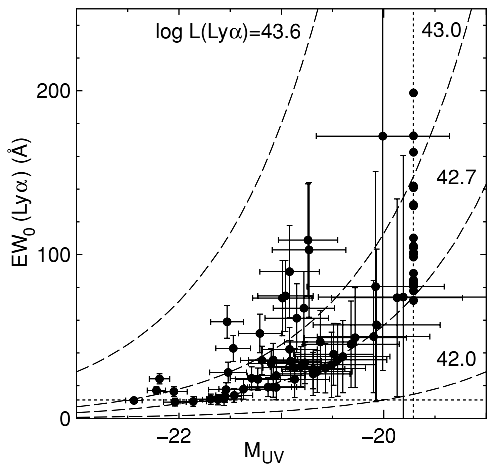

Figure 10.